QUANTIFICATION OF MEMBRANE IHC STAINS THROUGH MULTI-SPECTRAL IMAGING

Mehrnoush Khojasteh, Rabab Ward, and Calum MacAulay

British Columbia Cancer Research Center, and University of British Columbia, Vancouver, BC, Canada

ABSTRACT

This work presents a fully automated approach to the quantification of the expression of antibodies in immunohistochemically stained tissue sections.

Conventional RGB imaging was compared to multispectral imaging in the analysis of membrane stained tissue sections with high complexity, i.e. clustered and overlapping cells, and co-localization of stains. Preliminary results on more than 1700 cells suggest that multi-spectral imaging outperforms RGB imaging, particularly in complex and hard to segment regions.

1. INTRODUCTION

Protein expression levels have a well-established role in the early diagnosis of cancerous tissue. In addition, in the recent years, research has shown that they may have uses beyond diagnosis only. They can create new cancer screening tools, inform the design of new treatments, monitor treatment's effectiveness, and predict patient's response to treatment. Ultimately, the actual practice of genetically based personalized medicine requires the efficient detection of protein expression levels on a cell by cell basis to allow the identification of clonal population of cells relevant to available treatment options. One approach for monitoring and quantifying the activity of proteins is to analyze their localization and the intensity of their activity in pathological tissues by using images of the tissue where the localization of proteins is highlighted by labeled antibodies, so that the protein activity intensity is related to the intensity of the stains. This procedure is called immunohistochemistry (IHC) [1].

The most common method of interpreting IHC has been manual (visual) inspection, usually by a pathologist. In general, expression of these biomarkers was scored on an ordinal 0 – 3 scale which in some cases was combined with a scored interpretation of the markers' overall distribution. At best, manual inspection is only semi-quantitative, reducing continuous biomarker expression to an ordinal scale. In order to improve reproducibility and objectivity of the results interpretation, IHC quantification methods through computerized image analysis have been developed. High throughput IHC analysis on tissue microarrays through whole slide imaging or virtual microscopy further signifies automated quantification of IHC [2].

Assessing the expression of the biomarker on a cell-by-cell basis requires the identification of the location of each cell. Typically, the nuclei in the IHC stained tissues are stained with a counter-stain (e.g. Hematoxylin) that allows the localization of nuclei. If the antibody is specific to nuclei, once the nuclei are identified, the remaining task would be to assess the relative amount of the antibody stain for each nucleus. But in case of cytoplasmic or membrane stains, in addition to the location of the nuclei, cellular boundaries need to be identified, so that the antibody can be attributed to the corresponding cell.

The bottleneck of all automated quantification on a cell by cell basis is the robust and precise identification of cell nuclei. What are needed are segmentation methods which can reliably separate touching and overlapping objects and do not require the user to set numerous parameters and thresholds. The performance of the nuclei segmentation is very much dependent on the complexity of the IHC image in terms of the tissue type and the degree of overlap and aggregation among the nuclei, and the contrast between the nuclei and background, which in term depends on the number and spectral characteristic of the stains used, the specificity of the antibody (e.g. some antibodies are known to look "muddy"), the experimental conditions and the quality of the fixed tissue section. This should be considered when comparing the reported performance of different segmentation methods.

In this work, we attempt to analyze lymphoma tumour tissue sections. We consider these cases to be of high complexity due to the considerable overlap between the nuclei, and occasionally high density and unspecific localization of antibody, which makes the identification and separation of nuclei so difficult that even manual identification of nuclei proves to be quite challenging.

Our approach is to acquire multispectral images of the IHC stained tissue section slides, and separate the contribution of each stain to the optical density of each pixel, to obtain concentration maps of both stains. We perform our developed analysis (including the separation of stains, nuclei finding, and antibody stain measurement) on conventional RGB images and on multi-spectral images, and compare the performances to examine how the choice of the imaging modality affects the final assessment of the antibody abundance.

2. MATERIALS AND METHODS

2.1. Dataset

The data demonstrated in this article consist of 5 tissue microarray cores, which are formalin fixed, paraffin embedded tissue sections of 5 micron thickness, immunohistochemically stained with DAB for CD8 (a membrane-based antibody), and counter-stained with Hematoxylin. The percentage of positive cells in the 5 images covers the range between 0% and 30%. The cores were imaged under microscope with 20X magnification, and multispectral illumination generated by OneLight Spectra System (OneLight Corp., Vancouver, BC, Canada). Multispectral illumination consisted of twelve narrow-band illumination profiles centered between 410 nm and 630 nm with a step size of 20 nm, and bandwidth at half maximum of 15 nm. Simulated RGB images were generated by adding up the images in the first five channels as the Blue channel, the 7^{th} to 11^{th} channels as the Green channel, and the last two channels as the Red channel.

Manual nuclei identification was performed by marking the centers of the nuclei on RGB images of representative areas containing a total of more than 1700 cells.

2.2. Methods

As the first step in the pipeline, the multispectral data cube is acquired through multispectral illumination provided by the tunable light engine, OneLight Spectra. The next steps are: 1) Blind spectral unmixing, to separate contributions of each stain to the optical density of each pixel, 2) finding the nuclei in the concentration map of the counter-stain generated in the previous step, and 3) approximating the boundary of cells with Voronoi tessellation and obtaining per-cell measurements of the antibody stain.

2.2.1. Separation of stains

Theoretically the counter-stain must be localized to nuclei, and the antibody stain must be localized to the cell membranes, so there shouldn't be any spatial overlap between the two stains. In practice though, neither stains are 100% specific, and more importantly, the finite thickness of the tissue section causes superposition of different cells, resulting in areas of co-localization of the stains.

Color deconvolution on RGB images was shown to perform better than other color segmentation methods for the separation of stains, provided that the RGB vectors are experimentally determined [3]. Color deconvolution presents a special case of linear spectral unmixing. Spectral unmixing is the procedure by which the measured spectrum of a mixed pixel is decomposed into a collection of constituent spectra, or components, and a set of corresponding concentrations, that indicate the proportion of each component present in the pixel. Linear unmixing is based on the assumption that the total detected signal for every wavelength channel can be expressed as a linear combination of the contributing components [4]. According to the Beer-Lambert law, the optical density of a sample consisting of multiple dyes is linearly dependent on each dye's concentration, and the dye's absorption coefficient. So, the linear unmixing model is applicable to the absorption images after the pixel intensities are converted to optical densities through the logarithmic transformation.

Typical solutions of the linear unmixing model require the user to hand-pick representative points in the tissue image to indicate "pure" dye spectra. Once the pure dye spectra are known the unconstrained least squares solution for the concentration profiles can be calculated based on the bilinear model. However one important constraint to be imposed is the non-negativity of both concentrations and pure spectra.

MCR-ALS (Multivariate Curve Resolution through Alternating Least Squares) with non-negativity constraint is one way of solving the linear unmixing model. The model can be expressed as:

$$D = CS^T + E$$

Where D is the multispectral image cube, C is the matrix of concentrations of the components, and S is the pure component spectra matrix, and E is the experimental error. MCR-ALS solves this model iteratively by an alternating least squares algorithm. Initial estimates of either the concentrations or the pure spectra profiles are needed as input to the algorithm. With the initial estimates of either the concentrations or the pure spectra profiles provided as input to the ALS algorithm, it starts by solving for the pure spectra profile (S) or the concentrations (C) through a non-negative least square optimization technique [5].

In order to eliminate the user intervention in finding the initial estimates, we used the method of pure variable selection (based on the SIMPLISMA algorithm [6]), which automatically finds the most representative points in the tissue image for the different components in the set. This method finds initial estimates that are very close to those that are interactively obtained from the image.

2.2.2. Identification of the Nuclei

Once the concentration maps of the stains are available, the concentration map of the counter-stain (in this case, Hematoxylin) is used for the identification of nuclei.

Our fully automated procedure for the segmentation of nuclei starts with an initial segmentation of nuclei through local gradient weighted average thresholding. For every window of pixels, the threshold is calculated as $T = \frac{\sum I \times G}{\sum G}$, where I is the pixel intensity and G is the pixel gradient calculated with a 3x3 Sobel operator. The summation is done for all the pixels in the window, and the threshold value computed in this way is assigned to the center pixel of the window. The window is then moved across the

image, and at each location the threshold for the center pixel in the window is calculated. To reduce the computational cost, the windows do not overlap. Finally, a bilinear interpolation is applied to these thresholds to find the threshold levels for all the pixels. A window size of 16 by 16 pixels was found to perform well in this work.

This initial segmentation results in many clustered objects and won't be precise. Next, we apply an implementation of the "edge relocation algorithm" originally suggested in [7]. The algorithm makes use of intensity information, edge magnitude information and both object and edge connectivity information and generates a closed contour precisely along the edge of the nucleus. Briefly the algorithm generates a potential edge mask around the boundary of the initial rough segmentation of the object. Pixels inside the initial edge mask belong to the object foreground based on the initial segmentation. Amongst these pixels, those who are connected to the edge mask and satisfy the criteria to be a potential edge pixel are added to the edge mask. These pixels are those with high gradient values, or with intensities close to the value of otsu's threshold for the region. This step results in the cluster to be broken apart into smaller objects. The algorithm then starts to conditionally "thin" the edge mask by sequentially removing the pixels with low gradient from the mask, provided that the connectivity of the object and the mask are maintained. The algorithm is run iteratively until no more objects can be divided furthermore, and every object's boundary has been refined.

As a final step, distance-based watershed segmentation is applied to the image to break apart any clusters of objects that may remain in the image.

2.2.3. Measurement of the antibody stain

A Voronoi tessellation is generated using the centers of all the nuclei that were identified in the previous step, so that every nucleus is associated with a Voronoi polygon that approximates its cell boundary [8]. By superimposing this tessellation on the concentration map of the antibody stain, the intensity of the stain in each polygon is calculated which represents the relative expression level of the antibody in that cell. These relative expression levels may be used as continuous measures of antibody expression. But if it is required to determine whether or not a cell is immune-positive or immune-negative, it can be done by setting thresholds on the average intensity of the Voronoi polygons corresponding to cells. One way of finding such thresholds is to pick a region in each microarray core that doesn't have any positive staining, and calculated the mean and standard deviation of the pixels in that region. For each cell, the mean intensity and standard deviation of pixels inside the corresponding Voronoi polygon in the antibody stain image is calculated. The threshold is then calculated as mean plus a user-determined factor times the standard deviation. The factor can be determined experimentally.

3. RESULTS

The multi-step analysis was performed on both the three-channel RGB images and the 12-channel multispectral images separately.

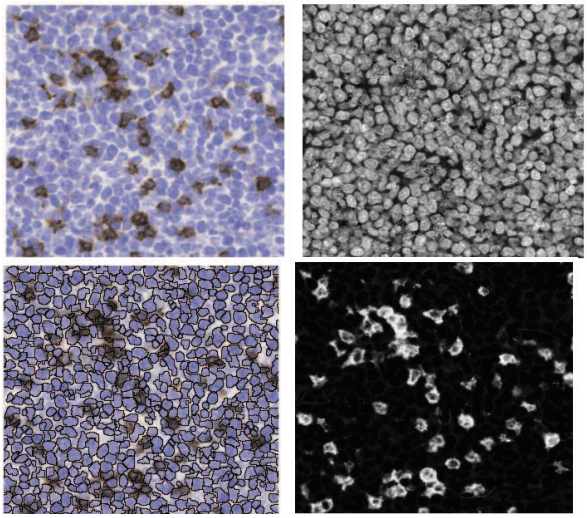


Figure 1. top left: the RGB equivalent of a sample image, top right: unmixed concentration map of Hematoxylin (nuclei image), bottom right: unmixed concentration of positive antibody stain, bottom left: final segmented nuclei

3.3. Linear spectral unmixing

The pure variable finding algorithm was able to completely eliminate user intervention in the spectral unmixing step. In every image, it was able to successfully identify the spectra of the purest pixels as the initial estimate of pure component spectra. The MCR-ALS algorithm refined the initial estimate to generate positive concentration maps. Figure 1 demonstrates one example of the unmixed Hematoxylin and DAB stains.

The unmixing results from the RGB images and multispectral images looked similar visually, but closer inspection showed that the RGB images do not allow complete unmixing of the stains, resulting in higher background intensity in both stain concentration maps.

3.4. Nuclei Segmentation

Nuclei segmentation was performed on both the RGB images, and the multispectral images. In the evaluation of the segmentation results, the focus was on finding the nuclei rather than finding the precise boundaries, because in our application, Voronoi maps based on nuclei centers are used to measure the antibody stain, and the exact boundary of the nuclei do not affect the final results. The performance of segmentation was evaluated through the ratio of the correctly identified nuclei. As mentioned earlier, the images were chosen so that they represent different ratios of positive staining, to allow for the evaluation of the analysis in different scenarios.

		Total No.	Correct	Missed	Over	Under	Percent Positive	total positve	true positive	false positive
Image 1	MSI	277	211 (76.2%)	12 (4.3%)	14 (5.1%)	40 (14.4%)	1.4%	4	100.0%	0.0%
	RGB		195 (70.4%)	19 (6.9%)	14 (5.1%)	49 (17.7%)			100.0%	25.0%
Image 2	MSI	588	424 (72.1%)	46 (7.8%)	30 (5.1%)	88 (15.0%)	9.4%	55	98.2%	9.1%
	RGB		397 (67.5%)	60 (10.2%)	68 (11.6%)	63 (10.7%)			98.2%	7.4%
Image 3	MSI	332	178 (53.6%)	47 (14.2%)	29 (8.7%)	78 (23.5%)	28.3%	94	96.8%	9.6%
	RGB		124 (37.3%)	99 (29.8%)	44 (19.6%)	65 (19.6%)			93.6%	7.7%
Image 4	MSI	277	206 (74.4%)	23 (8.3%)	5 (1.8%)	43 (15.5%)	7.6%	21	95.2%	0.0%
	RGB		164 (59.2%)	38 (13.7%)	19 (6.9%)	56 (20.2%)			95.2%	5.0%
Image 5	MSI	282	185 (65.6 %)	21 (7.4%)	28 (9.9%)	48 (17.0%)	25.9%	73	89.0%	8.2%
	RGB		126 (44.7%)	50 (17.7%)	35 (12.4%)	71 (25.2%)			89.0%	6.2%
Overall	MSI	1756	1204 (68.6%)	149 (8.5%)	106 (6.0%)	297 (16.9%)	14.1%	247	94.7%	8.1%
	RGB		1006 (57.3%)	266 (15.1%)	180 (10.3%)	304 (17.3%)			93.5%	7.3%

Table 1. Comparison of performance of RGB and Multi-spectral imaging (MSI), Over: over-segmented nuclei (one nucleus segmented into many pieces), under: under segmented nuclei (several nuclei segmented as one nucleus).

We found that for both the RGB images, and the multispectral images, the performance of the segmentation decreased with increasing antibody staining. The reason is that due to the non-ideal unmixing of the stains, the concentration map of the counter-stain in a region with strong antibody stain, doesn't have a high contrast between the nuclei. This was more pronounced in the RGB results. In all images, multispectral imaging resulted in better segmentation performance than RGB imaging. Table 1 summarizes the segmentation performance results.

3.5. Assessment of antibody stain

Both RGB images, and multispectral images performed well in this step. In order to evaluate the performance of the two imaging methods in determining the immune-positive and immune-negative cells, we generated the Voronoi tessellation based on the center of the manually found nuclei. We then superimposed this tessellation once on the on the stain map from the RGB images, and once on the stain map from the multispectral images, and each time measured the antibody stain inside each Voronoi polygon. In this way, we assumed a perfect segmentation, and only evaluated the performance of each method in generating a stain concentration map for the measurement of antibody stain.

The two imaging techniques resulted in equally good identification of the positive and negative cells. True positive and false positive rates are summarized in Table 1.

4. DISCUSSION AND CONCLUSION

We presented a fully-automated multi-step analysis approach to the quantification of antibody staining in high complexity immunostained tumour tissue sections. We demonstrated the performance of the approach on a set of more than 1700 cells on five images with different ratios of antibody staining ranging from very low staining to nearly 30% positive staining. Multispectral imaging outperformed the RGB imaging in all cases in terms of segmentation performance.

Even though these results need to be validated in a bigger dataset to enable statistically significant conclusions, they suggest that multispectral imaging may be more costly in terms of time, memory, and price, but the improvement in the segmentation results justifies the additional cost, particularly in highly complex images.

We found that due to imperfect stain separation, the regions with positive antibody stain have more under-segmented objects (clusters of cells). Future work includes use of the antibody stain image as an aid in the segmentation of nuclei in the counter-stain image, because the positive membrane staining in the cell membrane around the nucleus can help in separating that cell from the neighboring cells.

5. REFERENCES

[1] A. Blokzijl et al. "profiling protein expression and proximity ligation as a tool for personalized medicine", J. of internal medicine, v. 268 (3), pp. 232–245, 2010

[2] M. Cregger, et al, "Immunohistochemistry and Quantitative Analysis of Protein Expression", Archives of Path. & Lab. Med., v. 130 (7), pp. 1026-30, 2006.

[3] A.C. Ruifrok, et al. "Comparison of quantification of histochemical staining by hue-saturation-intensity transformation and color-deconvolution," Appl. Immunohistochem. Mol. Morphol., v. 11, pp. 85-91, 2003.

[4] N. Keshava et al. "Spectral unmixing", *Signal Processing Magazine, IEEE,* v. 19, pp. 44-57, 2002.

[5] A de Juan, et al. "Multivariate curve resolution (MCR) from 2000: Progress in concepts and applications", Critical reviews in anal. Chem.. v. 36, pp. 163-176, 2006

[6] W. Windig et al. "Interactive self-modeling mixture analysis", Anal. Chem. 63, pp. 1425-32, 1991.

[7] C. MacAulay and B. Palcic, "An edge relocation segmentation algorithm", Analytical and Quantitative Cytology and Histology, v. 12, pp. 165, 1990.

[8] F. Aurenhammer, "Voronoi Diagrams, A Survey of a Fundamental Geometric Data Structure," *ACM Computing Surveys,* v. 23, 1991.